ARTICLE
PUBLISHED ONLINE: 27 APRIL 2015 | DOI: 10.1038/NCHEMBIO.1800

nature chemical biology

HIV gp41–mediated membrane fusion occurs at edges of cholesterol-rich lipid domains

Sung-Tae Yang[1,2], Volker Kiessling[1,2], James A Simmons[2,3], Judith M White[2,3] & Lukas K Tamm[1,2]*

Lipid rafts in plasma membranes have emerged as possible platforms for the entry of HIV and other viruses into cells. However, little is known about how lipid phase heterogeneity contributes to viral entry because of the fine-grained and still poorly understood complexity of biological membranes. We used model systems mimicking HIV envelopes and T cell membranes and found that raft-like liquid-ordered (L_o-phase) lipid domains were necessary and sufficient for efficient membrane targeting and fusion. Interestingly, membrane binding and fusion were low in homogeneous liquid-disordered (L_d-phase) and L_o-phase membranes, indicating that lipid phase heterogeneity is essential. The HIV fusion peptide preferentially targeted to L_o-L_d boundary regions and promoted full fusion at the interface between ordered and disordered lipids. L_d-phase vesicles proceeded only to hemifusion. Thus, we propose that edges but not areas of raft-like ordered lipid domains are vital for HIV entry and membrane fusion.

Biological membranes that separate different compartments within cells or separate the cytosol from the extracellular space are composed of a broad variety of lipids, proteins and cholesterol. Depending on their location in the cell, membranes can have diverse lipid compositions, the roles of which are still not well understood. From the early fluid mosaic model[1], a much more detailed picture has emerged that describes biological membranes as complex, heterogeneous, asymmetric lipid-bilayer assemblies that are highly crowded with proteins[2,3]. The lipids in bilayer membranes not only differ in chemical identity but also occur in different thermodynamic states. The term 'lipid raft' was coined for certain specialized lipid microenvironments that are enriched in sphingolipids and cholesterol[4,5]. Lipid rafts have been implicated in a variety of dynamic cellular processes that influence membrane fluidity, serving as organizing centers for membrane-mediated cell signaling and regulating the activity of membrane proteins[6]. In addition, it has been suggested that lipid rafts have key roles in membrane fusion and fission[7,8], and increasing evidence indicates that lipid rafts serve as platforms for viral entry[9,10].

Viruses must overcome membrane barriers to deliver the viral nucleocapsid into the cytoplasm. A key step in the entry of enveloped viruses is the fusion of viral membrane envelopes with host membranes[11]. Direct viral fusion with the plasma membrane and endocytic pathways have been documented for HIV internalization[12,13]. The mechanism of viral membrane fusion is a well-studied process[14]. The structures and functions of a number of viral fusion proteins have been characterized to varying degrees of detail[15]. In the case of HIV entry, the gp120 subunit of the viral envelope spike glycoprotein gp120–gp41 first binds to CD4 on the target cell surface. This binding leads to conformational changes within gp120 that allow its additional binding to the CXCR4 or CCR5 coreceptor. A subsequent conformational change in the gp41 subunit exposes its N-terminal fusion peptide and causes it to be inserted into the cell membrane. An extended intermediate of gp41 then folds back on itself into a hairpin structure, in a process that brings the opposing membranes into close apposition in preparation for membrane fusion[16–18].

In addition to proteins, lipids have critical and cooperative roles in the process of membrane fusion during HIV entry[19]. Glycoproteins gp41 and gp120 and their receptors and coreceptors are thought to be associated with lipid rafts in the viral envelope and in target cell membranes, respectively[20]. Virus infection is inhibited after treatment of cell and viral membranes with methyl-β-cyclodextrin (MβCD), which extracts cholesterol and thus disrupts lipid rafts in these membranes[21]. Cholesterol depletion does not affect the virus's ability to bind target cells, but it significantly impairs viral entry[10]. This implies that rafts are likely to have an important role in membrane fusion. However, how cholesterol and associated lipid structures contribute to the mechanism of viral membrane fusion remains to be elucidated.

Lipid rafts are difficult to visualize directly in living cell membranes because of their small size (10–200 nm), their highly dynamic and perhaps transient nature and their own heterogeneity, all of which make their study difficult and controversial[6]. Some of these limitations can be overcome under controlled conditions in model membrane systems[22,23]. In a quest to understand the effects that lipid heterogeneity and rafts might have on the mechanism of viral membrane fusion, we used model membranes with complex lipid mixtures that mimicked those of the HIV envelope and T cell membranes, as well as additional, typical lipid mixtures with coexisting liquid-ordered (L_o) and liquid-disordered (L_d) phases, and we studied their effects on membrane fusion mediated by the HIV fusion peptide (FP). In these studies we used a version of the FP with a solubilizing C terminus, which allowed us to deliver the hydrophobic peptides to the fusing membranes from aqueous environments[24,25], as would occur in the full-length protein under physiological conditions. To corroborate our findings, we also examined the targeting of HIV pseudoviruses to structured membranes.

We show that the model membranes exhibited cholesterol-dependent raft-like lipid domains and that the HIV FP induced membrane fusion of phase-separated lipid bilayers containing such domains more efficiently than it did fusion of single-phase bilayers in either the L_o or the L_d state. The HIV FP and pseudotyped HIV interacted preferentially with boundaries between coexisting L_o and L_d lipid phases, and membrane fusion occurred preferentially at these domain boundaries. The results suggest that the edges of lipid rafts have a pivotal role in HIV entry, serving not only as the preferred docking sites but also as the preferred sites for the opening of fusion pores.

[1]Department of Molecular Physiology and Biological Physics, University of Virginia, Charlottesville, Virginia, USA. [2]Center for Membrane Biology, University of Virginia, Charlottesville, Virginia, USA. [3]Department of Cell Biology, University of Virginia, Charlottesville, Virginia, USA. *e-mail: Lkt2e@virginia.edu

RESULTS

HIV FP–mediated fusion requires ordered lipid domains

HIV and T cell membranes are composed of various phospholipids and cholesterol, with cholesterol/phospholipid molar ratios of about 0.8 in HIV membranes and about 0.4 in T cell membranes[26]. We first examined how fusion, measured by lipid mixing between liposomes prepared from lipid mixtures that mimicked the HIV envelope (HIV lipids: 33.1% sphingomyelin (SM), 16.0% phosphatidylcholine (PC), 35.2% phosphatidylethanolamine (PE), 15.5% phosphatidylserine (PS) and 0.2% other phospholipids, modeled here with corresponding proportions of porcine brain lipid species) and liposomes prepared from lipid mixtures that mimicked the T cell membrane (T cell lipids: 10.4% SM, 43.0% PC, 32.9% PE, 7.4% PS and 6.3% other phospholipids, modeled here with corresponding proportions of porcine brain lipid species), was promoted by HIV FP in the presence or absence of cholesterol. HIV FP induced rapid and efficient lipid mixing between HIV and T cell lipid liposomes when they contained their natural complements of 0.8 and 0.4 mol/mol cholesterol, respectively (**Fig. 1a**). However, fusion was considerably reduced when cholesterol was omitted from the HIV or the T cell lipid liposomes, or both. Supported HIV and T cell lipid monolayers stained with the membrane marker rhodamine-B-phosphoethanolamine (Rh-PE) are shown in **Supplementary Figure 1**. In the absence of cholesterol, the HIV lipids had large star-shaped domains, which are typical for gel-L_d phase coexistence[23]. The addition of cholesterol generated round domains, which are typical for L_o-L_d phase coexistence. The fraction of L_o-phase domains increased proportionally with the cholesterol concentration. These results indicate that raft-like L_o-phase domains promoted optimal lipid mixing (**Fig. 1a**). The results are also in good agreement with studies showing that HIV cell entry requires cholesterol and typical raft lipids for efficient fusion between the virus envelope and T cell membranes[10,21].

Next, we reproduced these studies with four simpler lipid compositions that are frequently used in model studies on the effects of lipid rafts and lipid phase behavior: liposomes composed of brain (b) SM, bPS and cholesterol (Ch) (2:1:1) (coexisting L_o and L_d phases) or of bSM and bPS (3:1) (coexisting gel and L_d phases), and single-phase bilayers composed of bPC and bPS (3:1) or of bPC, bPS and Ch (2:1:1) (**Fig. 1b** and **Supplementary Fig. 2**). The phase behavior of the lipid mixtures is shown in **Figure 1c–f**. Consistent with the results obtained with HIV and T cell lipid mixtures, HIV FP induced the most rapid and efficient fusion of L_{o+d}-phase bilayers.

To determine whether phase separation in the host or target lipid bilayer was responsible for the enhancement of fusion, we pre-incubated unlabeled liposomes composed of bPC and bPS (3:1) with HIV FP and added them to fluorescent-labeled liposomes composed of bSM, bPS and Ch (2:1:1) or bPC and bPS (3:1). HIV FP induced lipid mixing with and content release from bSM-bPS-Ch (2:1:1) liposomes, but not from bPC-bPS (3:1) liposomes (**Fig. 1g,h**). Increasing concentrations of cholesterol or bSM in rafts promoted fusion (**Fig. 1i,j**). Similarly, depletion of cholesterol in bilayers composed of bSM, bPS and Ch (2:1:1) with MβCD decreased fusion (**Fig. 1k**) and reduced the appearance of lipid rafts in supported bilayers (**Fig. 1l**). These results further support the notion that cholesterol-rich L_o-phase lipid domains are required for efficient HIV FP–mediated membrane fusion. Bilayers composed of bSM, dipalmitoyl PS (DPPS) and Ch (2:1:1) that formed a homogeneous L_o (without a coexisting L_d) phase with slow lipid lateral diffusion did not promote HIV FP–mediated fusion, whereas when we replaced the saturated chain DPPS with unsaturated chain di-oleoyl PS (DOPS) in an otherwise identical lipid mixture, L_o-phase domains formed and fusion was promoted (**Supplementary Fig. 3**).

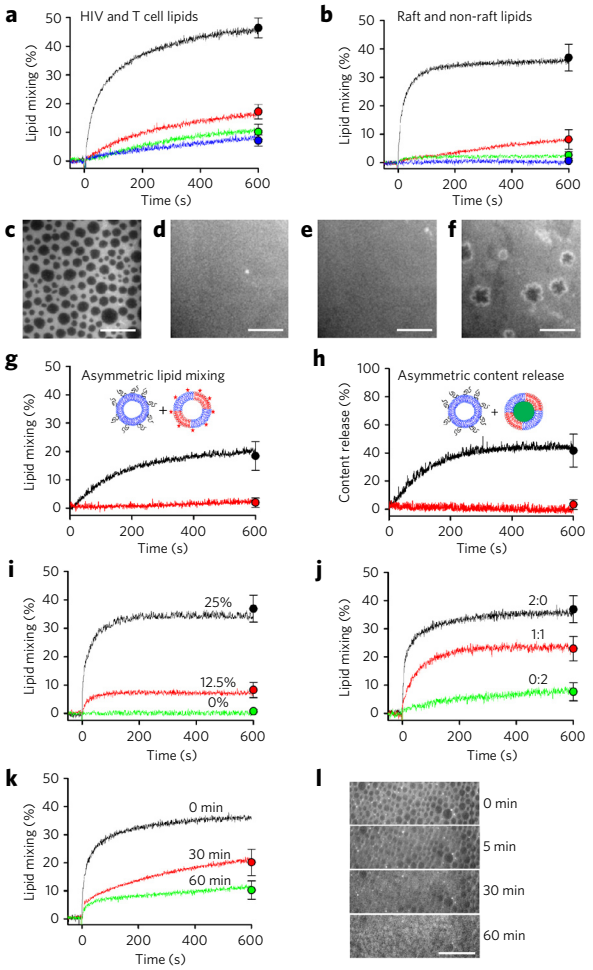

Figure 1 | Phase-separated domains and cholesterol are required for HIV FP to fuse HIV envelope– and T cell membrane–mimicking lipid mixtures. (**a**) HIV FP–mediated lipid mixing of a 1:9 mixture of HIV liposomes labeled with 1% NBD-PE and 1% Rh-PE and unlabeled T cell liposomes (black line). See text for lipid compositions of liposomes. In the absence of cholesterol, fusion was greatly reduced in HIV liposomes (red line), T cell liposomes (green line) or both (blue line). (**b**) HIV FP–mediated fusion of liposomes composed of bSM-bPS-Ch (2:1:1) (black line), bPC-bPS-Ch (2:1:1) (red line), bPC-bPS (3:1) (green line) and bSM-bPS (3:1) (blue line). (**c–f**) Fluorescence micrographs of 0.1 mol% Rh-PE–stained supported bilayers composed of bSM-bPS-Ch (2:1:1) (**c**), bPC-bPS-Ch (2:1:1) (**d**), bPC-bPS (3:1) (**e**) and bSM-bPS (3:1) (**f**). Scale bars, 20 μm. (**g**) 45 μM unlabeled bPC-bPS (3:1) liposomes were pre-incubated with HIV FP and then added to 5 μM NBD-PE–Rh-PE–labeled liposomes composed of bSM-bPS-Ch (2:1:1) (black line) or bPC-bPS (3:1) (red line). (**h**) Same as **g**, but with liposomes labeled with the polyanionic fluorophore ANTS and the cationic quencher DPX. (**i**) HIV FP–mediated fusion of bSM-bPS (2:1) HIV FP–incubated liposomes with 0% (green line), 12.5% (red line) and 25% (black line) cholesterol. (**j**) HIV FP–mediated fusion of liposomes composed of bSM-bPC-bPS-Ch in molar ratios of 0:2:1:1 (green line), 1:1:1:1 (red line) and 2:0:1:1 (black line). Ratios above lines are ratios of SM to PC in each type of liposome. (**k**) HIV FP–mediated fusion of bSM-bPS-Ch (2:1:1) liposomes before treatment (black line) and after 30-min (red line) or 60-min (green line) treatment with 5 mM MβCD. (**l**) Representative fluorescence micrographs of the same area of a supported bSM-bPS-Ch (2:1:1) bilayer at the indicated times after the addition of 5 mM MβCD. Scale bar, 10 μm. Total liposome concentrations were 50 μM in all experiments, and the FP concentration was 2 μM, except in **a**, where it was 1 μM. In **a**, **b** and **g–k**, colored circles with error bars denote mean ± s.d., with colors defined as for lines in each panel. Data are representative of three experiments.

HIV FP interacts preferentially with domain boundaries

We reasoned that the increased fusion activity with two-phase ordered-disordered bilayers was the result of increased binding of HIV FP to such membranes. To test this notion, we used total internal reflection fluorescence (TIRF) microscopy on supported bPC-bPS (3:1) bilayers with prebound HIV FP to capture liposomes with different phase properties (**Fig. 2a**). Liposomes composed of bSM, DOPS and Ch (2:1:1, L_{o+d} phases) were captured much more efficiently than liposomes composed of bPC and bPS (3:1, pure L_d phase) or bSM, DPPS and Ch (2:1:1, pure L_o phase) (**Fig. 2b**). Representative TIRF images of each type of liposome bound to the supported bilayers are shown in **Figure 2c–e**. In addition, when we added L_d or L_o liposomes together with equal amounts of L_{o+d} liposomes in competition experiments, the L_{o+d} liposomes bound preferentially to the HIV FP–doped supported membranes (**Fig. 2f–h**).

To determine to which regions of a two-phase lipid bilayer HIV FP membranes would bind, we turned the configuration of our supported-membrane TIRF experiment around as shown in **Figure 2i** and used double-label fluorescence microscopy to colocalize liposome binding with different membrane phases. Liposomes composed of bPC and bPS (3:1) and labeled with the lipophilic tracer DiD were pre-incubated with HIV FP and then bound to a two-phase supported bilayer composed of bSM, bPS and Ch (2:1:1) that was stained with Rh-PE. The phase structures of the supported bilayer and the bound liposomes were visualized with epifluorescence and TIRF microscopy, respectively (**Fig. 2j,k**). The overlay showed that most liposomes bound to the boundaries between L_d- and L_o-phase lipid domains (**Fig. 2l**). Quantification of HIV FP–targeted liposomes in the different regions of the two-phase bilayer showed that ~5 (1.5) times more liposomes bound to domain boundaries than to L_d (L_o) regions (**Supplementary Fig. 4**).

To assess whether the targeting of HIV FP liposomes is specific to the sequence of HIV FP, we performed similar experiments with the FP of influenza hemagglutinin. Influenza virus enters cells by receptor-mediated endocytosis and requires the low pH of the endosome for fusion and FP insertion into the membrane[27]; therefore, these experiments were carried out at pH 5. The binding of liposomes to coexisting L_{o+d} supported bilayers mediated by the influenza FP showed no preference for the L_o-L_d boundary region over the L_o or L_d regions of the membrane (**Supplementary Fig. 5**). Clearly, the HIV FP was more selective for the phase boundary region than the influenza FP was (**Supplementary Fig. 5d**). The lower pH was not responsible for this difference, as the HIV FP still bound to phase boundaries at pH 5. Considering that the endosomal membrane contains less cholesterol than the plasma membrane and is not known to harbor lipid rafts, the indifference of the influenza FP to raft phase boundaries is physiologically sensible.

HIV FP LUVs bind to GUV domain boundaries

To generalize our finding of HIV FP–mediated domain-boundary targeting of large unilamellar vesicles (LUVs) with supported membranes, we examined the same behavior with giant unilamellar vesicles (GUVs)[28]. We pre-incubated DiD-labeled LUVs composed of bPC and bPS (3:1) with HIV FP and allowed them to bind to Rh-PE–labeled GUVs with the following compositions: bSM, DOPC and Ch (2:2:1) for two-phase L_{o+d} bilayers (**Fig. 3a–c**), bPC only for uniform L_d-phase bilayers (**Fig. 3d–f**), and bSM and Ch (2:1) for uniform L_o-phase bilayers (**Fig. 3g–i**). After 30 min of incubation, numerous bright spots were observed in the DiD channel, indicating that many LUVs had bound to the GUVs in an HIV FP–dependent manner (**Fig. 3b**). No such interactions were observed in the absence of HIV FP. Overlaying the images in **Figure 3a,b** revealed that most LUVs bound to the domain boundaries of the GUVs composed of bSM, DOPC and Ch (**Fig. 3c**). HIV FP–targeted LUVs were not observed on the surface of the single-phase GUVs composed of either bPC or bSM-Ch (**Fig. 3e,h**). The image of another GUV

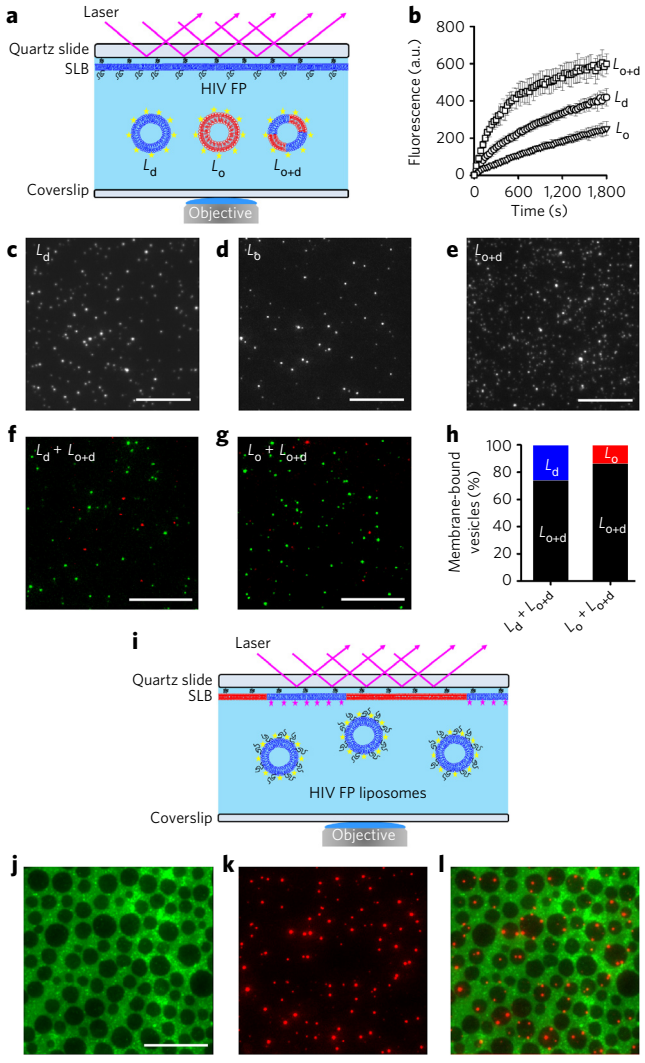

Figure 2 | Membrane-bound HIV FP preferentially binds phase-separated L_{o+d} liposomes and targets L_o-L_d phase boundaries in phase-separated membranes. (**a**) Schematic of TIRF microscopy approach used to measure the binding of liposomes to supported membranes pre-incubated with HIV FP. SLB, supported lipid bilayer. (**b**) Time course of mean fluorescence intensity recorded by TIRF microscopy measuring the binding of bPC-bPS (3:1, L_d), bSM-DPPS-Ch (2:1:1, L_o) and bSM-DOPS-Ch (2:1:1, L_{o+d}) liposomes to HIV FP–doped supported bilayers. Data are representative of three experiments. (**c–e**) TIRF micrographs of bound L_d (**c**), L_o (**d**) and L_{o+d} (**e**) liposomes captured 10 min after liposome addition. (**f,g**) Competitive binding of two types of liposomes to HIV FP–doped supported bilayers. L_d and L_{o+d} liposomes (0.2 μM each) (**f**) or L_o and L_{o+d} liposomes (0.2 μM each) (**g**) were added to the supported membranes. Green spots indicate L_{o+d} liposomes labeled with 0.1 mol% Rh-PE, and red spots indicate L_d or L_o liposomes labeled with 0.5 mol% DiD. In **c–g**, scale bars represent 20 μm. (**h**) Quantitative analysis of bound fraction of each type of liposome in **f** and **g**. (**i**) Schematic of TIRF microscopy approach used to determine the locations of HIV FP–targeted liposomes in different regions of supported two-phase bilayers composed of bSM-bPS-Ch (2:1:1). Liposomes composed of bPC-bPS (3:1) were pre-incubated with HIV FP and then allowed to bind to the supported membrane. (**j**) Epifluorescence micrograph of supported membrane stained with 0.1 mol% Rh-PE. (**k**) TIRF micrograph of bound 0.5 mol% DiD-labeled liposomes as mediated by HIV FP. (**l**) Overlay image showing that most liposomes favored the boundaries between L_d and L_o phases (also see **Supplementary Fig. 4**). In **j–l**, scale bars represent 20 μm.

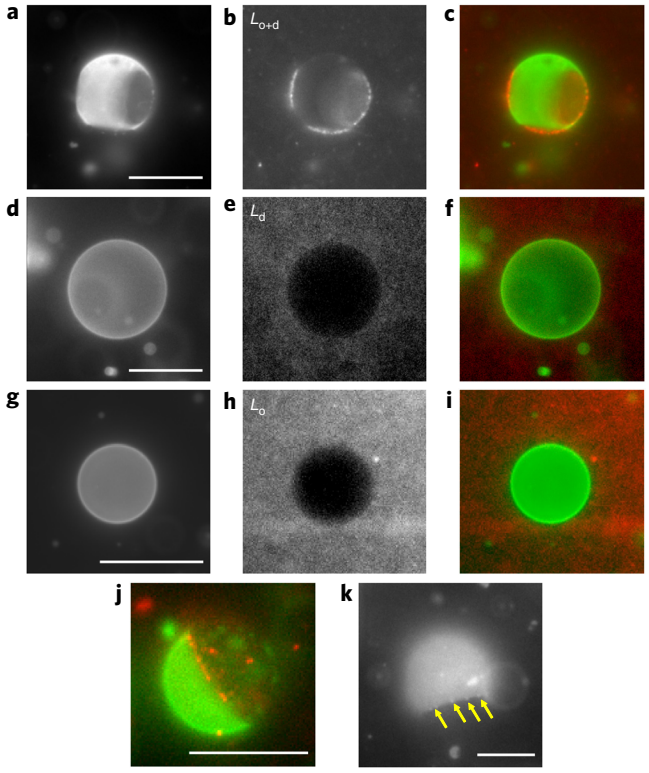

Figure 3 | HIV FP liposomes are targeted to L_o-L_d phase boundary regions in GUVs. (**a**–**i**) Fluorescence micrographs of GUVs labeled with 0.1 mol% Rh-PE (**a**,**d**,**g**) and LUV liposomes labeled with 0.5 mol% DiD (**b**,**e**,**h**). GUVs were composed of bSM-DOPC-Ch (2:2:1) for L_{o+d} (**a**–**c**), bPC for L_d (**d**–**f**) and bSM-Ch (2:1) for L_o (**g**–**i**) phase bilayers. LUVs were composed of bPC-bPS (3:1) and were pre-incubated for 10 min with HIV FP before they were added to the GUVs. Images were taken after 30 min of incubation at room temperature. Images in **c**, **f** and **i** are two-color overlays of the other panels in the same row. (**j**) Fluorescence micrograph showing HIV FP–mediated binding of LUVs to the phase boundary region of an L_{o+d} phase-separated GUV membrane. The overlay shows GUV phase behavior in green and the bound LUVs in red. (**k**) Fluorescence micrograph of HIV FP LUVs bound to the phase boundary region of a phase-separated L_{o+d} GUV membrane. In this experiment, LUVs and GUVs were labeled with Rh-PE for simultaneous observation. Several bright spots representing LUVs (indicated by yellow arrows) were concentrated at a domain boundary. Scale bars, 20 μm (in **a**–**i**, scale bar in leftmost panel applies to all panels in that row).

again showed that most LUVs were bound at the phase domain boundary on the L_{o+d} GUV surface (**Fig. 3j**). When the GUVs and LUVs were both labeled with Rh-PE, we could simultaneously monitor fluctuating dynamic domain boundaries on the GUV surface and the relative positions of LUVs bound to these boundaries (**Supplementary Video 1**). The LUVs (**Fig. 3k**) moved along the L_o-L_d boundaries on the GUV, indicating that the HIV FP–bound LUVs remained confined to the boundary, even if this line was moving on the vesicle.

An *N*-(7-nitro-2,1,3-benzoxadiazol-4-yl) (NBD)-labeled HIV FP analog also bound preferentially to two-phase LUVs and GUVs (**Supplementary Fig. 6**). As explained in the **Supplementary Results**, the peptides remained bound to their original liposomes and did not migrate from one liposome to another. When the HIV FP was bound to GUVs, long lipid tubules grew out from the L_o-L_d boundary regions (**Supplementary Fig. 7**). Similar effects were not observed on single-phase L_d or L_o GUVs. Although interesting, this tubulation process was not investigated further in this study.

HIV FP liposomes fuse at L_o-L_d phase boundaries

Having observed that HIV FP liposomes preferentially targeted L_o-L_d phase boundaries, we wanted to know whether these boundaries were also the sites of fusion. To explore this, we prepared Rh-PE–labeled supported bilayers composed of bSM, bPC and Ch (2:2:1), which mimicked the outer leaflet of host cell membranes, and used TIRF microscopy to observe individual fusion events[29] of DiD-labeled liposomes composed of HIV lipids (L_{o+d} mixture as in **Figs. 1a** and **4a**–**c**), bSM-DOPS-Ch (2:1:1, standard L_{o+d} mixture; **Fig. 4d**–**f**), bPC-bPS (3:1, L_d mixture; **Fig. 4g**–**i**) or bSM-DPPS-Ch (2:1:1, L_o mixture; **Fig. 4j**–**l**). The supported membranes were pre-incubated with HIV FP before the liposomes were added. Although all four types of liposomes bound to domain boundaries on the supported membranes as expected, only the two-phase L_{o+d} liposomes (**Fig. 4a**–**f**) fused efficiently with the supported membrane, whereas the single-phase L_d and L_o liposomes did not (**Fig. 4g**–**l**). In these experiments, fusion was observed when DiD from the vesicles mixed with the supported membrane[29], which resulted in a rapid spread and equilibration into the L_d regions and a more readily observable, slower spread of growing round fluorescent domains in the L_o-phase domains (**Supplementary Video 2** and **Supplementary Fig. 8**).

We analyzed ~4,400 individual liposome fusion events by plotting peak fluorescence intensities from individual liposomes as a function of time. We noted three distinct behaviors of fluorescence intensity: no change with time (**Fig. 4m**), complete decay (**Fig. 4n**) and decay to around one-half of the original peak intensity (**Fig. 4o**). We assigned these behaviors to docking, full fusion and hemifusion events, respectively. Selected TIRF images of the time evolution of individual liposomes were used to visualize each behavior (**Fig. 4m**–**o**). To further prove that the liposomes with the behavior shown in **Figure 4n** were indeed undergoing full fusion, we prepared DiD-labeled liposomes, which we also loaded with the water-soluble fluorescent dye sulforhodamine B in order to measure content release upon fusion[30]. Two-phase supported bilayers composed of bSM, bPC and Ch (2:2:1) were labeled with NBD-DPPE, which preferentially partitions into the L_o phase[23], and lipid mixing and the release of sulforhodamine B from fusing HIV lipid liposomes were tracked by following the fluorescence intensities in and around individual liposomes. The three-color experiment presented in **Figure 4p** shows that the content dye of an L_{o+d} liposome that bound to a domain edge and hemifused at time 0 was released upon full fusion (after 32.2 s) into the space under the supported membrane, providing direct proof for complete membrane fusion. The sulforhodamine B signal decreased approximately exponentially over a period of 3.8 s, which can be explained only by a graded release through a fusion pore and is inconsistent with vesicle rupture, which would have resulted in dissipation of the fluorescence from its origin within milliseconds. This process is shown in **Supplementary Video 3**.

The relative frequencies of the different types of events shown in **Figure 4m**–**o** are plotted in **Figure 4q**. Although similar numbers of the different types of liposomes (1,307 for HIV lipids, 1,182 for L_{o+d}-phase liposomes, 1,062 for L_d-phase lipids, and 903 for L_o-phase lipids) were analyzed for fusion on supported membranes, HIV FP did not induce fusion of liposomes in the L_o phase, and only 18% of liposomes in the L_d phase showed membrane fusion, including hemifusion. In contrast, 72% ± 6% of the HIV lipid and 64% ± 7% of the model L_{o+d} liposomes that fused were bound at domain boundaries. Therefore, phase coexistence in both the target and the liposome membrane was required for efficient membrane fusion to occur.

Activated HIV Env pseudoviruses target domain boundaries

To test whether HIV particles would also target phase boundaries in heterogeneous target membranes, we prepared murine leukemia virus particles pseudotyped with HIV-1 envelope protein and

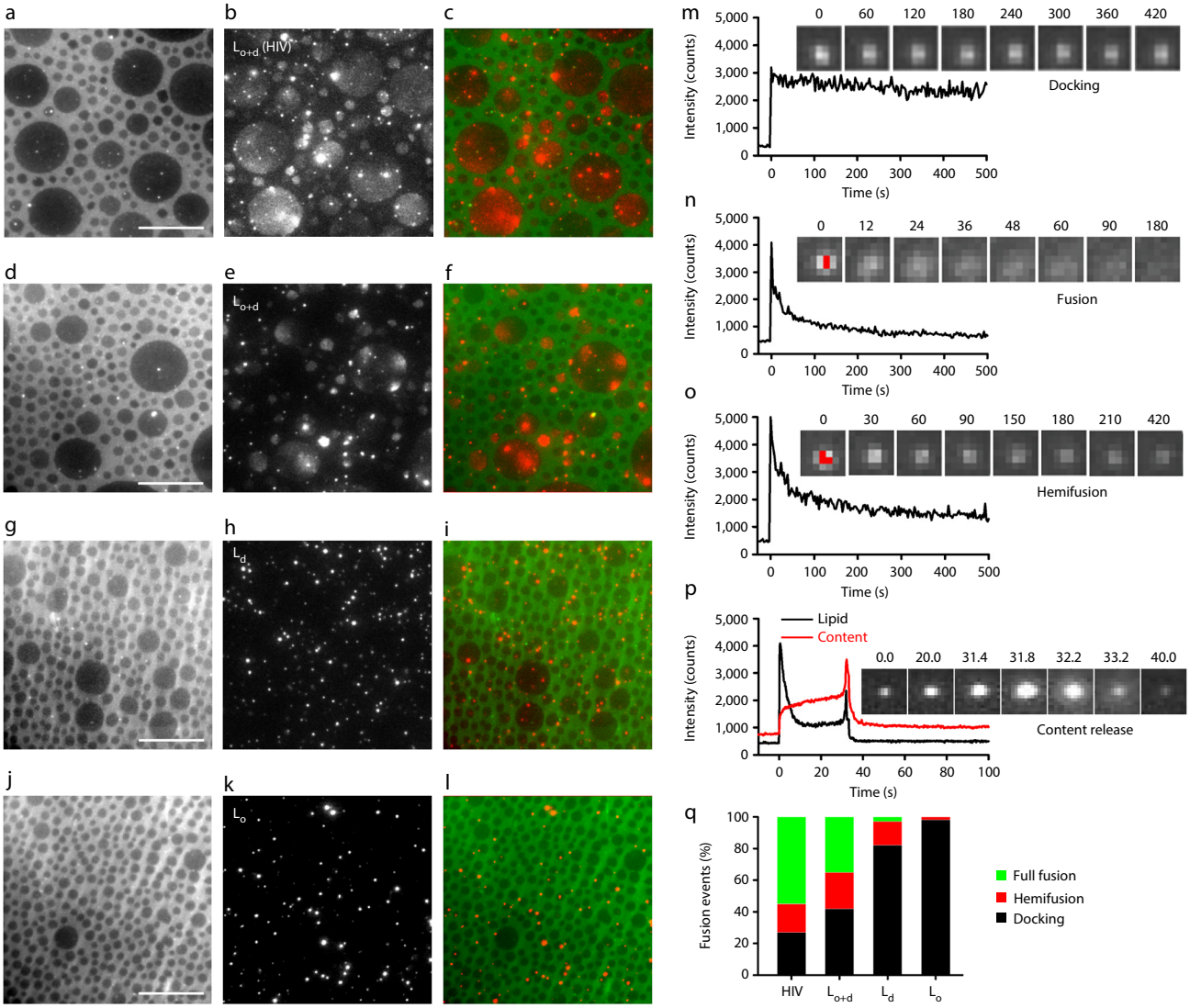

Figure 4 | HIV FP liposomes fuse at L_o-L_d phase boundaries in supported membranes. (**a**–**l**) Rh-PE–labeled supported bilayers composed of bSM-bPC-Ch (2:2:1) (**a**,**d**,**g**,**j**) were incubated with 5 μM HIV FP for 10 min. DiD-labeled liposomes composed of HIV lipids (**b**) or of bSM-DOPS-Ch (2:1:1) (**e**) for L_{o+d}, bPC-bPS (3:1) (**h**) for L_d or bSM-DPPS-Ch (2:1:1) (**k**) for L_o bilayers were added and observed by TIRF microscopy. The overlayed images (**c**,**f**,**i**,**l**) show that L_{o+d} liposomes (red) (**c**,**f**), but not L_d or L_o liposomes (**i**,**l**), fused with supported bilayers (green). Representative of three experiments. Scale bars, 20 μm (in each row, the scale bar in the leftmost panel applies to all panels in that row). (**m**–**o**) Different typical fluorescence behaviors of single bound liposomes: constant fluorescence corresponding to binding without fusion (docking) (**m**), complete fluorescence decay corresponding to full fusion (**n**) and fluorescence decay to ~50% of the original, corresponding to hemifusion (**o**). Time zero was defined as the first frame with a visible liposome. TIRF images of single liposomes at representative times (in seconds) are shown along the top of each panel (size represented: 2.5 × 2.5 μm^2). See text for details on evaluated events. (**p**) Fluorescence time course of a single DiD- and sulforhodamine B–labeled liposome. Binding and lipid spread (black line) and content release (red line) were recorded simultaneously in respective channels. We tracked content release by integrating the fluorescence intensity from the vesicle area. The insets show TIRF images of content release from the liposome at representative times (in seconds). Size represented in insets: 5 × 5 μm^2. (**q**) Relative frequencies of different events: binding without fusion (docking), hemifusion and full fusion.

investigated their binding to phase-separated membranes composed of bSM, DOPC and Ch (2:2:1). Because in native gp120 and gp41 the fusion peptide is buried within the envelope protein, and as no receptors were included in the target membrane, little binding of HIV pseudoviruses to these membranes was observed. However, when the envelope glycoprotein was activated by mild heat and enfuvirtide treatment to expose the FP, strong binding to the boundaries between L_o and L_d phases was observed in supported bilayers (**Fig. 5a–c**) and GUVs (**Fig. 5d–f**). Quantification of the data shown in **Figure 5a–c** and statistics that include additional repeat experiments are presented in **Supplementary Table 1**. Enfuvirtide is known to stabilize the activated structure of gp41 that features an exposed FP by interfering with the formation of the fusion-promoting helical hairpin between heptad regions 1 and 2 of gp41 (ref. 31). As there was little binding of HIV pseudoviruses to the membranes in the absence of heat or enfuvirtide activation, the viruses' preferential binding to the boundary regions was most likely mediated by the FP of gp41.

DISCUSSION

In this work we developed a molecular understanding of why cholesterol and cholesterol-induced lipid phase heterogeneity in membranes are important for the insertion of the FP of HIV gp41 and its ability to fuse membranes. Although lipid rafts in cell membranes

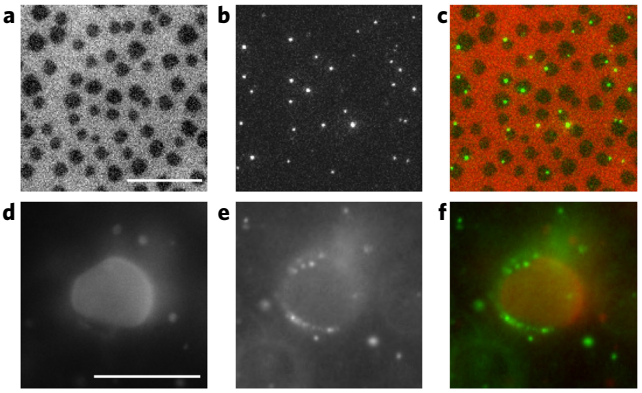

Figure 5 | HIV-1 pseudoviruses bind preferentially to L_o-L_d phase boundaries in supported lipid bilayers or GUVs composed of bSM-DOPC-Ch (2:2:1). (**a**–**f**) Fluorescence micrographs of a supported bilayer (**a**–**c**) and a GUV (**d**–**f**) labeled with 0.1 mol% DiD (**a**,**d**) and HIV pseudoviruses labeled with the viral-content marker gag-mKO (**b**,**e**). Images in **c** and **f** are two-color overlays of the other images in their respective rows. HIV pseudoviruses were pre-incubated with enfuvirtide at 55 °C for 30 min and then added to both lipid bilayers. Images of membrane-bound HIV pseudoviruses were taken after 30 min of incubation at room temperature. The overlays show the preferential binding of the HIV particles to the L_o-L_d boundary regions of the phase-separated membranes. Scale bars, 20 μm (scale bar in **a** applies to **b** and **c**; scale bar in **d** applies to **e** and **f**). Representative of three experiments.

and the high concentration of cholesterol in HIV envelopes have long been implicated as important factors contributing to cell entry, the molecular reasons for their requirement were not well understood. This is not surprising because lipid rafts are still ill defined in terms of lipid composition, size and longevity, and there is mounting evidence that many kinds of different raft-like structures coexist in cell membranes. This unsatisfactory situation prompted us to take a reconstitution approach to develop *in vitro* model membranes with complex but well-controlled and well-defined lipid configurations. This approach allowed us to study the effects of many different lipids in the context of structured lipid bilayers expected to mimic those encountered in cell membranes, but at larger length scales that were amenable to investigation by optical microscopy. Using a combination of supported and liposomal model membranes, we were able to observe previously unknown molecular interactions of the HIV FP with membrane constituents that were organized in complex fabrics resembling those of cell membranes and define supramolecular requirements for the promotion of membrane fusion that would be difficult to observe by other means.

The HIV FP promoted the most efficient fusion between liposomes containing lipid mixtures that separate into coexisting ordered and disordered phases, such as those present in the HIV envelope and target T cell membranes. We found that for efficient fusion, it was more important to have lipid phase separation in the target membrane than in the host (viral) membrane. Ordered or disordered single-phase target membranes fused less easily than two-phase membranes, even if they contained equal amounts of cholesterol. This proves that cholesterol is necessary, but not sufficient, for fusion, and that its context with other lipids matters in promoting efficient fusion.

The reason for fusion promotion in two-phase membranes can be traced to our finding that liposomes decorated with the HIV FP preferentially targeted L_o-L_d phase boundaries in supported lipid bilayers and GUVs. Both systems essentially yielded the same results, but there are some technical differences between them. The GUV system has the advantage that possible adverse effects of the quartz support that may occur in supported-bilayer experiments are eliminated. As domain boundaries are mobile in GUVs, we were also able to use epifluorescence microscopy to follow bound liposomes as they moved with the domain boundaries. In contrast, supported bilayers are planar, permitting the acquisition by TIRF microscopy of much larger sets of data and statistics for quantifying the liposome-boundary interactions.

We found that HIV FP–decorated liposomes not only bound to L_o-L_d phase boundaries but also fused preferentially at those boundaries. Fusion to pure L_o- and L_d-phase membranes was much less frequent. Our single-liposome fusion assay also allowed us to distinguish between full and hemifusion events. Quite interestingly, we found that HIV FP–promoted fusion resulted in mostly hemifusion events with pure L_d-phase target membranes, whereas full fusion was prevalent at the L_o-L_d phase boundaries.

Although our experiments were carried out at room temperature, they are highly relevant to situations at 37 °C. Nanoscale lipid rafts are observed in living cell membranes at physiological temperatures[32], and raft-like domains persist in model membranes up to physiological temperatures[33]. Critical fluctuations are observed at temperatures a few degrees below 37 °C in model membranes and plasma membrane–derived vesicles[34,35], and these lipid heterogeneities are stabilized to persist to at least 37 °C by adhesion and interactions with the cytoskeleton[36,37]. This behavior makes interfaces between ordered and disordered lipids even more prevalent in these systems than in neatly phase-separated bilayers. Therefore, our finding that HIV gp41 prefers interfaces between ordered and disordered lipids for entry by membrane fusion would be at least as relevant at 37 °C as observed here at room temperature.

We recognize that HIV FP–mediated fusion might not capture the full story of fusion mediated by the entire gp120 or gp41 fusion protein. HIV FP insertion into target membranes occurs only after binding of gp120 to its receptor and coreceptor. There is no question that additional factors such as the distribution of the envelope protein in the viral envelope and the distribution of receptors and coreceptors on the host cell membranes may have additional, significant roles in the selection of appropriate sites for fusion in complex target membranes. However, as discussed by many, raft-like lipid assemblies in cell membranes may be very small, perhaps even as small as a few dozen lipid molecules[7,38]. This would make interfaces between such lipid clusters much more frequent in cell membranes than in model membranes and might make these interfaces much easier to reach from any location in the membrane. However, the guiding physical principles for FP insertion, membrane bending and, ultimately, fusion would be the same as visualized here in the reconstituted lipid systems that demonstrated phase separations on larger, optically resolvable length scales.

Figure 6 illustrates possible connections of domain-boundary targeting in the biological system (**Fig. 6a**) and in the reduced-lipid model-membrane system with just the HIV FP as the fusogen (**Fig. 6b**,**c**). When HIV binds to its receptors on the cell membrane and gets activated for fusion, gp41 extends from a raft-like viral envelope in a pre-hairpin conformation in which the FPs are projected toward the target membrane (**Fig. 6a**; also see ref. 18). The CD4 receptor and the chemokine coreceptors are also thought to be recruited to lipid rafts in the host cell membrane, and the binding of HIV would therefore bring ordered lipid domains of the virus and host cell membranes into close proximity. The interaction of the FP with a phase boundary in the host membrane leads to three possible configurations of virus–host membrane contacts: L_d-boundary, L_o-boundary and boundary-boundary (**Fig. 6b**). Our results showed that the boundary-boundary contact provided the most efficient configuration for membrane fusion, whereas fusion in the other configurations proceeded only to hemifusion (L_d-boundary) or was virtually not observed (L_o-boundary).

Why are lipid domain boundaries beneficial for membrane fusion? Membrane fusion costs energy: membranes need to bend,

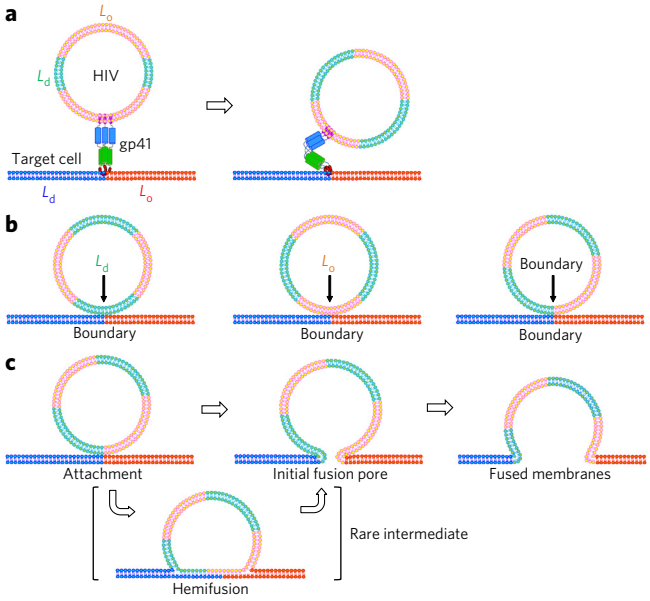

Figure 6 | Lipid domain boundaries in viral and cellular target membranes promote HIV gp41–mediated membrane fusion. (**a**) Targeting of HIV particles to domain boundaries of two-phase lipid bilayers. The exposed fusion peptides of gp41 in the triggered pre-hairpin intermediate interact with the domain boundaries of the target cell membrane. (**b**) Three possible configurations of L_o-L_d lipid bilayer attachments: L_d-boundary (left), L_o-boundary (center) and boundary-boundary (right). Membrane fusion is most efficient in the boundary-boundary attachment configuration. (**c**) Proposed mechanism of membrane fusion at L_o-L_d lipid domain boundaries. The boundary-boundary attachment configuration lowers the energy required to open the initial fusion pore, which later expands to a fully fused membrane. Hemifusion intermediates are sometimes seen in this configuration. They may be caused by lipid asymmetry of the host membrane– and viral membrane–derived hemifusion diaphragm. In this model, the hemifusion state is resolved by shifting of phase-mismatched leaflets back into register, which leads to opening of the initial fusion pore.

water needs to be removed between the two fusing membranes and lipids need to assume non-bilayer conformations, all of which are energetically disfavored in single-phase lipid bilayers. The energy required to drive membrane fusion is thought to be provided by the refolding of the fusion protein and by the insertion of the FPs into the host bilayer. The boundaries between different lipid phases are the favored sites for FP insertion and also probably present 'fault lines' for membrane deformations. Specifically, (1) FPs preferably insert at the edges of raft domains, where they probably also self-associate into larger oligomeric structures[39,40], as they are always delivered in multiples of three because of the trimeric structure of the fusion protein; (2) lipid mismatch at L_o-L_d interfaces, which is likely to be asymmetric because of the one-sided insertion of the FPs, induces membrane curvature and thereby reduces the free energy of curved membrane fusion intermediates; (3) the topological discontinuity at the interface between L_o and L_d phases creates line tension[41,42], which may be relieved and provide energy upon membrane fusion; (4) the boundary-boundary contact across two lipid bilayers is energetically favorable[43,44] and may lead to favorable domain coalescence between these bilayers, which could promote membrane fusion; and (5) lipid asymmetries between viral and target membranes can favor hemifusion intermediates requiring shifting of mismatched domain boundaries between the two leaflets back into register, which would promote full fusion. A progression of membrane fusion at lipid domain boundaries is illustrated in **Figure 6c**.

The effects of lipid rafts and especially raft domain boundaries on HIV FP–mediated membrane fusion described in this work might not be limited to this particular fusion system, and in fact might be much more general. Lipid phase heterogeneity and edge effects of lipid rafts have recently been shown to change current thinking about how lipidated signaling molecules such as Rac1 are translocated to membranes[45]. Membrane discontinuities at the edges of rafts may affect membrane fusion in the entry pathways of not only HIV but also other enveloped viruses, and they might play a role in intracellular vesicle fusion in membrane trafficking in healthy cells. Cholesterol-dependent lipid and protein clusters—in lipid raft or non-raft associations—have been implicated in neurotransmitter release at synapses[46], neuronal SNARE protein assemblies[47], the formation of multinucleated myotubes[48] and osteoclasts[49] and sperm-egg cell fusion[50]. It will be interesting to see to what other fusion systems the conclusions of this work can be extended to in the future. The tools that we have developed here should facilitate many exciting future investigations of lipid-domain edge effects in viral and non-viral membrane fusion.

Received 4 December 2014; accepted 25 March 2015; published online 27 April 2015

METHODS

Methods and any associated references are available in the online version of the paper.

References

1. Singer, S.J. & Nicolson, G.L. The fluid mosaic model of the structure of cell membranes. *Science* **175**, 720–731 (1972).
2. Engelman, D.M. Membranes are more mosaic than fluid. *Nature* **438**, 578–580 (2005).
3. Kiessling, V., Wan, C. & Tamm, L.K. Domain coupling in asymmetric lipid bilayers. *Biochim. Biophys. Acta* **1788**, 64–71 (2009).
4. Simons, K. & Ikonen, E. Functional rafts in cell membranes. *Nature* **387**, 569–572 (1997).
5. Brown, D.A. & London, E. Functions of lipid rafts in biological membranes. *Annu. Rev. Cell Dev. Biol.* **14**, 111–136 (1998).
6. Pike, L.J. The challenge of lipid rafts. *J. Lipid Res.* **50** (suppl.), S323–S328 (2009).
7. Jacobson, K., Mouritsen, O.G. & Anderson, R.G.W. Lipid rafts: at a crossroad between cell biology and physics. *Nat. Cell Biol.* **9**, 7–14 (2007).
8. Baumgart, T., Hess, S.T. & Webb, W.W. Imaging coexisting fluid domains in biomembrane models coupling curvature and line tension. *Nature* **425**, 821–824 (2003).
9. Campbell, S.M., Crowe, S.M. & Mak, J. Lipid rafts and HIV-1: from viral entry to assembly of progeny virions. *J. Clin. Virol.* **22**, 217–227 (2001).
10. Liao, Z., Cimakasky, L.M., Hampton, R., Nguyen, D.H. & Hildreth, J.E. Lipid rafts and HIV pathogenesis: host membrane cholesterol is required for infection by HIV type 1. *AIDS Res. Hum. Retroviruses* **17**, 1009–1019 (2001).
11. White, J.M., Delos, S.E., Brecher, M. & Schornberg, K. Structures and mechanisms of viral membrane fusion proteins: multiple variations on a common theme. *Crit. Rev. Biochem. Mol. Biol.* **43**, 189–219 (2008).
12. Wilen, C.B., Tilton, J.C. & Doms, R.W. Molecular mechanisms of HIV entry. *Adv. Exp. Med. Biol.* **726**, 223–242 (2012).
13. Melikyan, G.B. HIV entry: a game of hide-and-fuse? *Curr. Opin. Virol.* **4**, 1–7 (2014).
14. Chernomordik, L.V. & Kozlov, M.M. Mechanics of membrane fusion. *Nat. Struct. Mol. Biol.* **15**, 675–683 (2008).
15. Harrison, S.C. Viral membrane fusion. *Nat. Struct. Mol. Biol.* **15**, 690–698 (2008).
16. Bartesaghi, A., Merk, A., Borgnia, M.J., Milne, J.L. & Subramaniam, S. Prefusion structure of trimeric HIV-1 envelope glycoprotein determined by cryo-electron microscopy. *Nat. Struct. Mol. Biol.* **20**, 1352–1357 (2013).
17. Julien, J.P. *et al.* Crystal structure of a soluble cleaved HIV-1 envelope trimer. *Science* **342**, 1477–1483 (2013).
18. Tamm, L.K., Lee, J. & Liang, B. Capturing glimpses of an elusive HIV gp41 prehairpin fusion intermediate. *Structure* **22**, 1225–1226 (2014).
19. Doms, R.W. & Moore, J.P. HIV-1 membrane fusion: targets of opportunity. *J. Cell Biol.* **151**, F9–F14 (2000).
20. Waheed, A.A. & Freed, E.O. Lipids and membrane microdomains in HIV-1 replication. *Virus Res.* **143**, 162–176 (2009).
21. Graham, D.R., Chertova, E., Hilburn, J.M., Arthur, L.O. & Hildreth, J.E. Cholesterol depletion of human immunodeficiency virus type 1 and simian immunodeficiency virus with beta-cyclodextrin inactivates and permeabilizes the virions: evidence for virion-associated lipid rafts. *J. Virol.* **77**, 8237–8248 (2003).

22. Dietrich, C. *et al.* Lipid rafts reconstituted in model membranes. *Biophys. J.* **80**, 1417–1428 (2001).
23. Crane, J.M. & Tamm, L.K. Role of cholesterol in the formation and nature of lipid rafts in planar and spherical model membranes. *Biophys. J.* **86**, 2965–2979 (2004).
24. Han, X. & Tamm, L.K. A host-guest system to study structure-function relationships of membrane fusion peptides. *Proc. Natl. Acad. Sci. USA* **97**, 13097–13102 (2000).
25. Tamm, L.K. & Han, X. Viral fusion peptides: a tool set to disrupt and connect biological membranes. *Biosci. Rep.* **20**, 501–518 (2000).
26. Brügger, B. *et al.* The HIV lipidome: a raft with an unusual composition. *Proc. Natl. Acad. Sci. USA* **103**, 2641–2646 (2006).
27. Tamm, L.K. Cell entry of influenza virus by membrane fusion. In *Influenza Viruses—Facts and Perspectives* (ed. Schmidt, M.F.G.) 48–55 (Grosse Verlag, 2007).
28. Feigenson, G.W. Phase behavior of lipid mixtures. *Nat. Chem. Biol.* **2**, 560–563 (2006).
29. Domanska, M.K., Kiessling, V., Stein, A., Fasshauer, D. & Tamm, L.K. Single vesicle millisecond fusion kinetics reveals number of SNARE complexes optimal for fast SNARE-mediated membrane fusion. *J. Biol. Chem.* **284**, 32158–32166 (2009).
30. Kiessling, V. *et al.* Rapid fusion of synaptic vesicles with reconstituted target SNARE membranes. *Biophys. J.* **104**, 1950–1958 (2013).
31. Kilby, J.M. *et al.* Potent suppression of HIV-1 replication in humans by T-20, a peptide inhibitor of gp41-mediated virus entry. *Nat. Med.* **4**, 1302–1307 (1998).
32. Eggeling, C. *et al.* Direct observation of the nanoscale dynamics of membrane lipids in a living cell. *Nature* **457**, 1159–1162 (2009).
33. de Almeida, R.F., Fedorov, A. & Prieto, M. Sphingomyelin/phosphatidylcholine/cholesterol phase diagram: boundaries and composition of lipid rafts. *Biophys. J.* **85**, 2406–2416 (2003).
34. Honerkamp-Smith, A.R. *et al.* Line tensions, correlation lengths, and critical exponents in lipid membranes near critical points. *Biophys. J.* **95**, 236–246 (2008).
35. Veatch, S.L. *et al.* Critical fluctuations in plasma membrane vesicles. *ACS Chem. Biol.* **3**, 287–293 (2008).
36. Zhao, J., Wu, J. & Veatch, S.L. Adhesion stabilizes robust lipid heterogeneity in supercritical membranes at physiological temperature. *Biophys. J.* **104**, 825–834 (2013).
37. Machta, B.B., Papanikolaou, S., Sethna, J.P. & Veatch, S.L. Minimal model of plasma membrane heterogeneity requires coupling cortical actin to criticality. *Biophys. J.* **100**, 1668–1677 (2011).
38. Edidin, M. The state of lipid rafts: from model membranes to cells. *Annu. Rev. Biophys. Biomol. Struct.* **32**, 257–283 (2003).
39. Lai, A.L., Moorthy, A.E., Li, Y. & Tamm, L.K. Fusion activity of HIV gp41 fusion domain is related to its secondary structure and depth of membrane insertion in a cholesterol-dependent fashion. *J. Mol. Biol.* **418**, 3–15 (2012).
40. Qiang, W. & Weliky, D.P. HIV fusion peptide and its cross-linked oligomers: efficient syntheses, significance of the trimer in fusion activity, correlation of beta strand conformation with membrane cholesterol, and proximity to lipid headgroups. *Biochemistry* **48**, 289–301 (2009).
41. Lipowsky, R. Domain-induced budding of fluid membranes. *Biophys. J.* **64**, 1133–1138 (1993).
42. Garcia-Sáez, A.J., Chiantia, S. & Schwille, P. Effect of line tension on the lateral organization of lipid membranes. *J. Biol. Chem.* **282**, 33537–33544 (2007).
43. Jensen, M.H., Morris, E.J. & Simonsen, A.C. Domain shapes, coarsening, and random patterns in ternary membranes. *Langmuir* **23**, 8135–8141 (2007).
44. Tayebi, L. *et al.* Long-range interlayer alignment of intralayer domains in stacked lipid bilayers. *Nat. Mater.* **11**, 1074–1080 (2012).
45. Moissoglu, K. *et al.* Regulation of Rac1 translocation and activation by membrane domains and their boundaries. *J. Cell Sci.* **127**, 2565–2576 (2014).
46. Chamberlain, L.H., Burgoyne, R.D. & Gould, G.W. SNARE proteins are highly enriched in lipid rafts in PC12 cells: implications for the spatial control of exocytosis. *Proc. Natl. Acad. Sci. USA* **98**, 5619–5624 (2001).
47. Murray, D.H. & Tamm, L.K. Clustering of syntaxin-1A in model membranes is modulated by phosphatidylinositol 4,5-bisphosphate and cholesterol. *Biochemistry* **48**, 4617–4625 (2009).
48. Mukai, A. *et al.* Dynamic clustering and dispersion of lipid rafts contribute to fusion competence of myogenic cells. *Exp. Cell Res.* **315**, 3052–3063 (2009).
49. Ishii, M. *et al.* RANKL-induced expression of tetraspanin CD9 in lipid raft membrane microdomain is essential for cell fusion during osteoclastogenesis. *J. Bone Miner. Res.* **21**, 965–976 (2006).
50. Sleight, S.B. *et al.* Isolation and proteomic analysis of mouse sperm detergent-resistant membrane fractions: evidence for dissociation of lipid rafts during capacitation. *Biol. Reprod.* **73**, 721–729 (2005).

Acknowledgments

This work was supported by NIH grants R01 AI30577 (to L.K.T.) and R21 AI103601 (to J.M.W.). We thank E. Nelson for technical help with the production of pseudoviruses.

Author contributions

S.-T.Y., V.K., J.M.W. and L.K.T. designed research; S.-T.Y. performed most experiments; J.A.S. provided pseudotyped viruses; S.-T.Y., V.K., J.M.W. and L.K.T. analyzed data; and S.-T.Y., V.K. and L.K.T. wrote the paper.

Competing financial interests

The authors declare no competing financial interests.

Additional information

Supplementary information is available in the online version of the paper. Reprints and permissions information is available online at http://www.nature.com/reprints/index.html. Correspondence and requests for materials should be addressed to L.K.T.

ONLINE METHODS

Materials. All lipids including fluorescent probes were from Avanti Polar Lipids (Alabaster, AL). The only exceptions were 1,1′-dioctadecyl-3,3,3′,3′-tetramethylindodicarbocyanine perchlorate (DiD), aminonaphthalene-1,3,6-trisulfonic acid (ANTS) and p-xylene-bis-pyridinium bromide (DPX), which were from Molecular Probes (Invitrogen, Carlsbad, CA). Cholesterol, MβCD and 4-chloro-7-nitrobenzofurazan (NBD-Cl) were purchased from Sigma (St. Louis, MO). 1,2-dimyristoyl-phosphatidylethanolamine-N-(polyethylene glycol-triethoxysilane) (DPS) and the HIV FP with the sequence AVGIGALFLGFLGAAGSTMGAASGGGKKKKK were custom synthesized by Shearwater Polymers (Huntsville, AL) and by the Yale W.M. Keck Biotechnology Resource Laboratory (New Haven, CT), respectively.

Preparation of liposomes. Large unilamellar vesicles (LUVs) were prepared via the extrusion technique. In brief, the desired amounts of lipids dissolved in chloroform or a mixture of chloroform and methanol were mixed, and the solvent was evaporated under a stream of nitrogen gas in a glass test tube. The lipid film was further dried under vacuum overnight and hydrated with 0.5 ml HEPES buffer (10 mM HEPES, 120 mM NaCl, pH 7.2). The resulting suspension was subjected to ten cycles of freezing and thawing using liquid nitrogen and warm water and then extruded 21 times through two stacked polycarbonate filters of 100-nm pore size (Avestin, Ottawa, ON). Giant unilamellar vesicles (GUVs) were prepared via the electroformation technique[51]. In brief, 25 µl of a 10 mM lipid solution in organic solvent containing the fluorescent lipid probe Rh-PE (0.1 mol%) was deposited on a clean glass slide that was coated with indium tin oxide, and the slide was then placed in vacuum for 90 min to eliminate residual solvent. A fabrication chamber filled with 300 mM sucrose in H_2O was composed of two conducting slides separated by a 0.5-mm spacer. We performed electroformation at around 60 °C by applying alternating electric current (3 V, 10 Hz) for 120 min. The GUVs were transferred into a 300 mM glucose solution and allowed to settle by gravity on the microscope slide.

Preparation of supported lipid monolayers and bilayers. Quartz slides (Quartz Scientific, Fairport Harbor, OH) were cleaned by boiling in Contrad detergent for 15 min and then sonicated for 30 min in a hot bath. After rinsing with water and ethanol, remaining organic residues were removed by Piranha solution (3:1 mix of 95% H_2SO_4 and 30% H_2O_2) and the slides were rinsed extensively in pure water. Lipid mixtures were spread onto a pure-water surface in a Nima 611 Langmuir-Blogdett trough (KSV NIMA, Espoo, Finland). Solvent was allowed to evaporate for 10 min at a surface pressure of 5 mN/m, and then the monolayer was compressed at a rate of 10 cm^2/min to reach a surface pressure of 32 mN/m. The quartz slides were further cleaned immediately before use for 10 min in an argon plasma sterilizer (Harrick Scientific, Ossining, NY) and were then dipped into the trough at a speed of 200 mm/min and withdrawn at 5 mm/min while the surface pressure was kept constant at 32 mN/m. This transferred a single lipid monolayer onto the quartz support. Polymer (PEG)-supported lipid bilayers were formed via a combined Langmuir-Blodgett (LB)–LUV fusion technique as previously described[52]. Each LB monolayer contained 3 mol% of the reactive lipid DPS, containing 77 ethylene glycol units, to link the polymer and lipid covalently to the SiO_2 surface of the quartz slide. The slide was dried in a vacuum desiccator at room temperature overnight and cured in a 70 °C oven for 40 min. After equilibration in a desiccator at room temperature, the slide with the tethered polymer-supported LB monolayer was placed in a custom-built flow-through chamber. A 0.1 mM suspension of LUVs in HEPES buffer was injected into the chamber and incubated for at least 2 h at room temperature. Excess LUVs in the chamber were washed out by extensive rinsing with HEPES buffer. Typically only the top monolayer contained 0.1 mol% Rh-PE or 0.5 mol% NBD-PE. Otherwise, and with the exception of DPS in the bottom monolayer, the lipid compositions of both leaflets were identical.

Binding of NBD-labeled HIV FP to vesicles. 1 mM HIV FP was reacted with 2 mM NBD-Cl in borate buffer (50 mM borate, 20 mM EDTA, pH 8.0) for 1 h at room temperature. Uncoupled dye was removed by gel filtration on a PD-10 column. To measure the binding of NBD-labeled peptides to LUVs with different lipid phases, we added the LUVs successively to 0.5 µM NBD-labeled HIV FP in HEPES buffer. The fluorescence emission spectra were recorded with a Jobin-Yvon Fluorolog-3 spectrofluorometer (Jobin-Yvon, Edison, NJ) with excitation at 475 nm, and the intensities at 530 nm were measured as a function of the lipid-to-peptide molar ratio. To visualize the binding of HIV FP to phase-separated GUVs, we incubated 1 µM NBD-labeled HIV FP at room temperature for 30 min with GUVs that were labeled with Rh-PE.

Liposome lipid mixing and content release induced by HIV FP. The lipid-mixing assay was based on a commonly used fluorescence resonance energy transfer assay[53]. LUVs were added to a cuvette in a ratio of 1:9 of labeled (1 mol% Rh-PE and NBD-PE each) to unlabeled LUVs to give a total lipid concentration of 50 µM in HEPES buffer at room temperature. Lipid mixing induced by HIV FP was recorded under constant stirring using a Fluorolog-3 spectrofluorometer with the excitation and emission wavelengths set at 460 nm and 535 nm, respectively. To measure content release, we prepared LUVs in a buffer solution containing the small water-soluble fluorescent dye ANTS together with the quencher DPX (12.5 mM ANTS, 45 mM DPX, 50 mM NaCl, 10 mM HEPES, pH 7.2). Unencapsulated dyes and quenchers were removed by size-exclusion chromatography with a PD-10 desalting column (Amersham Biosciences, Piscataway, NJ). Content release induced by the HIV FP was recorded under constant stirring using the Fluorolog-3 spectrofluorometer with the excitation and emission wavelengths set at 355 nm and 520 nm, respectively. The 0% lipid-mixing and content-release marks were the fluorescence intensities of the LUV suspension before HIV FP was added, and the 100% levels of lipid mixing and content release were defined by the fluorescence intensities produced after the addition of 0.5% (vol/vol) Triton X-100 to the reactions.

Visualization of HIV FP–mediated binding of LUVs to GUVs. To visualize the binding of LUVs to GUVs mediated by the HIV FP, we labeled GUVs with 0.1 mol% Rh-PE and LUVs with 0.5 mol% DiD. HIV FP was incubated with LUVs (peptide:lipid molar ratio of 1:50) for 10 min and then injected into the chamber containing the GUVs. The binding of LUVs to GUVs was monitored by epifluorescence microscopy. Images were recorded on a Zeiss Axiovert 200 fluorescence microscope (Carl Zeiss, Thornwood, NY) with a mercury lamp as a light source, a 63× water-immersion objective (Carl Zeiss; 0.95 NA) and an electron-multiplying charge-coupled device (EMCCD) cooled to −70 °C (iXon DV887ESC-BV, Andor, Belfast, UK) as a detector. Images were acquired using homemade software written in LabVIEW (National Instruments, Austin, TX). Bilayers stained with NBD were illuminated through a 480-nm band-pass filter (D480/30, Chroma, Brattleboro, VT) and via a dichroic mirror (505dclp, Chroma) through the objective. Fluorescence was observed through a 535-nm band-pass filter (D535/40, Chroma). Rhodamine-stained bilayers were illuminated through a 540-nm band-pass filter (D540/25, Chroma) and via a dichroic mirror (565dclp, Chroma) through the objective. Fluorescence was observed through a 605-nm band-pass filter (D605/55, Chroma). LUVs stained with DiD were illuminated through a 620-nm filter (ET620/60, Chroma) and via a dichroic mirror (660dclp, Chroma) and were observed through a 665-nm band-pass filter (HQ665/60, Chroma). All images were obtained at room temperature.

Visualization and quantification of HIV FP–mediated binding of LUVs to supported lipid bilayers. To measure the efficiency of binding of LUVs to supported lipid bilayers mediated by the HIV FP, we incubated the bilayers with 5 µM HIV FP for 10 min at room temperature, after which unbound peptides were washed away with HEPES buffer. 2 µmol of LUVs labeled with 0.5 mol% DiD were added to the supported membranes. To investigate the targeting of LUVs to different regions of L_d-L_o phase-separated supported membranes, we labeled the LUVs and bilayers with 0.5 mol% DiD and 0.1 mol% Rh-PE, respectively. HIV FP was incubated with LUVs (peptide:lipid molar ratio of 1:50) for 10 min and then injected into the chamber with the supported membrane. To monitor the binding of LUVs to the supported bilayer by TIRF microscopy, we directed a focused laser beam (CUBE 640-40C, Coherent, Palo Alto, CA) through a trapezoidal prism onto the quartz-buffer interface where the supported bilayer was attached. The prism-quartz interface was lubricated with glycerol to allow easy translation of the sample chamber on the microscope stage. The laser beam was totally internally reflected at an angle of 72° from the surface normal, producing an evanescent wave that decayed exponentially in the solution with a characteristic penetration depth of 90 nm. The intensity of the laser beam was modulated by the computer or could be completely blocked by a computer-controlled shutter (Vincent Associates, Rochester, NY). Images were recorded by an EMCCD (iXon DV887ESC-BV, Andor). Data acquisition and image analysis from TIRF microscopy were accomplished through custom-built software written in LabVIEW (National Instruments,

doi:10.1038/nchembio.1800

Austin, TX)[54]. To analyze and quantify the distribution of membrane-bound liposomes, we distinguished three regions of the supported membranes: L_o domains, L_d phase areas, and boundary regions with a 0.75-µm width centered on the perimeter of each L_o domain. Custom-built particle-tracking software[54] was used to automatically detect the position (*x*- and *y*-coordinate) of each liposome

HIV FP–mediated fusion of single liposomes to supported lipid bilayers. To monitor fusion of single liposomes with supported lipid bilayers, we incubated the supported membranes with 5 µM HIV FP for 10 min at room temperature and then washed away unbound peptides with HEPES buffer. 2 µmol of LUVs labeled with 0.5 mol% DiD were added to the supported membranes. To monitor content mixing, we prepared LUVs in a buffer solution containing water-soluble fluorescent sulforhodamine B (10 mM HEPES, 50 mM sulforhodamine B, pH 7.2, adjusted to 250-mmol/kg osmolality by addition of NaCl). We removed unencapsulated dye by running the liposomes through a PD-10 desalting column. Docking and fusion of individual liposomes to the supported membrane were monitored by TIRF microscopy using a diode laser (CUBE640, Coherent) and an argon-ion laser (Innova 90C-5, Coherent) at the same time[30]. Single fusion events were analyzed as described[29,30].

Binding of HIV pseudovirus to phase-separated membranes. Viral particles pseudotyped with a murine leukemia virus (MLV) core and the HIV-1 envelope protein were prepared by cotransfection of 293T cells with 3 µg pFB-Luc (reporter plasmid), 2 µg pHIT60 (MLV-gag-Pol), 1 µg MLV gag-mKO (a gift from G. Melikyan) and 3 µg HIV-1 JRFL Env plasmids per 10-cm culture dish. Viral supernatants were harvested 48 h after transfection and centrifuged at 2,500 rpm for 10 min at 4 °C. They were flash-frozen and stored at −70 °C for later use. Supported lipid bilayers or GUVs composed of bSM-DOPC-Ch (2:2:1) were labeled with 0.1 mol% DiD. The viruses were incubated for 30 min at 55 °C in the presence of 10 µg/ml enfuvirtide (Sigma, St. Louis, MO) and brought back to room temperature. After equilibration at room temperature, the viruses were added to supported bilayers or GUVs. The heat and enfuvirtide treatments were omitted in control experiments. mKO-labeled HIV pseudoviruses were illuminated through a 540-nm band-pass filter (D540/25, Chroma) and dichroic mirror (565dclp, Chroma) through the objective, and fluorescence was observed through a 605-nm band-pass filter (D605/55, Chroma). Supported lipid bilayers and GUVs stained with DiD were illuminated through a 620-nm filter (ET620/60, Chroma) and via a dichroic mirror (660dclp, Chroma) and were observed through a 665-nm band-pass filter (HQ665/60, Chroma).

51. Angelova, M.I. & Dimitrov, D.S. Liposome electroformation. *Faraday Discuss. Chem. Soc.* **81**, 303–311 (1986).
52. Wagner, M.L. & Tamm, L.K. Tethered polymer-supported planar lipid bilayers for reconstitution of integral membrane proteins: silane-polyethyleneglycol-lipid as a cushion and covalent linker. *Biophys. J.* **79**, 1400–1414 (2000).
53. Struck, D.K., Hoekstra, D. & Pagano, R.E. Use of resonance energy transfer to monitor membrane fusion. *Biochemistry* **20**, 4093–4099 (1981).
54. Kiessling, V., Crane, J.M. & Tamm, L.K. Transbilayer effects of raft-like lipid domains in asymmetric planar bilayers measured by single molecule tracking. *Biophys. J.* **91**, 3313–3326 (2006).